Materials Chemistry and Physics 145 (2014) 99–107

Contents lists available at ScienceDirect

Materials Chemistry and Physics

journal homepage: www.elsevier.com/locate/matchemphys

A theoretical and experimental exploration of the mechanism of microwave assisted 1,3-dipolar cycloaddition of pyridinium ylides to single walled carbon nanotubes

Mustafa K. Bayazit [a,*], Nihat Celebi [b], Karl S. Coleman [a]

[a] Department of Chemistry, University of Durham, Durham DH1 3LE, UK
[b] Department of Chemistry, Abant Izzet Baysal University, Bolu 14280, Turkey

HIGHLIGHTS

- PM3 (RHF) type calculations suggest that charges are probably transferred from HOMO of pyridinium ylides to LUMO of SWNTs.
- Theoretical predictions indicate a $HOMO_{ylide}$–$LUMO_{(8,8)\ SWNT}$ controlled 1,3-DC reaction (Type I).
- Pyridinium ylides with smaller HOMO–LUMO energy gap is experimentally found to be more selective to large diameter SWNTs.
- Reactivity of pyridinium ylide might be manipulated using strong electron withdrawing groups.
- Graphene surface modification may be anticipated using the same approach.

GRAPHICAL ABSTRACT

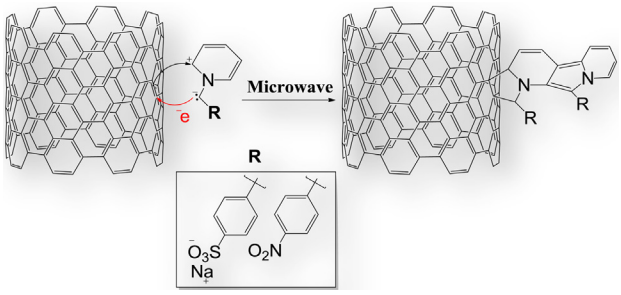

ARTICLE INFO

Article history:
Received 5 August 2013
Received in revised form
13 January 2014
Accepted 22 January 2014

Keywords:
Nanostructures
Chemical synthesis
Computational techniques
Organic compounds

ABSTRACT

Cycloaddition reactions have widely been used for surface functionalization of single walled carbon nanotubes (SWNTs). Here, 1,3-dipolar cycloaddition (1,3-DC) of two new pyridinium ylides, generated *in-situ* via the addition of triethylamine (NEt_3) to the Kröhnke salts *N*-(4-methyl sodium benzene sulfonate)-pyridinium bromide and *N*-(4-nitrobenzyl)-pyridinium bromide, to SWNTs under microwave conditions are assessed both theoretically using PM3 (RHF) type calculations and experimentally. Evidence of covalent surface modification is provided by FTIR, UV–vis–NIR and resonance Raman spectroscopy. Solubility of the modified SWNTs increases when compared to as-received SWNTs. Quantification of surface groups is performed via TGA-MS and XPS. 1,3-DC of pyridinium ylides with smaller HOMO–LUMO energy gap is found to be more selective to large diameter SWNTs. Theoretically predicted smaller energy gaps between $HOMO_{ylides}$ and $LUMO_{(8,8)}$ SWNT suggest that the charges are probably transferred from pyridinium ylides to SWNTs indicating $HOMO_{ylide}$–$LUMO_{(8,8)\ SWNT}$ controlled 1,3-DC. Regioselectivity of second ylide addition as addendum to ylide–SWNT adduct is also discussed.

1. Introduction

Carbon nanotubes (CNTs) have gained increasingly more scientific attention in nanoscience due to their exceptional electrical,

* Corresponding author. Current address: Department of Chemistry, Imperial College London, South Kensington Campus, London SW7 2AZ, UK. Tel.: +44 (0)20 7589 5111.
E-mail address: m.bayazit@imperial.ac.uk (M.K. Bayazit).

0254-0584
http://dx.doi.org/10.1016/j.matchemphys.2014.01.045

thermal and mechanical properties and might find application in areas diverse as composite materials, energy storage, sensors, field emission devices and nanoscale electronic components [1,2]. However, the poor solubility of raw material both in aqueous and organic medium is an issue while being processed. Covalent surface modification of CNTs enhances the solubility and processability of them together with offering possible reactive functional side groups for further applications and separation [3–8]. Covalent functionalization strategies including 1,3-dipolar cycloadditions (1,3-DCs) to sort CNTs in terms of their helicity and diameter has recently been reviewed [9,10]. The use of 1,3-DCs has also been extended to the covalent surface modification of graphene [11,12]. Practicality of 1,3-DCs of a series of 1,3-dipoles to armchair SWNTs (5,5) was theoretically examined and, versatility of using azomethine ylides, ozone, nitrile ylides and nitrile imines were also predicted theoretically [13]. In agreement with the solid-state physics description of band structures [14], electronic structure and chemical reactivity of carbon nanotubes were also described using real-space orbital representations and traditional concepts of aromaticity, orbital symmetry and frontier orbital [15]. Experimentally, azomethine ylides, typically generated *in-situ* by the thermal condensation of aldehydes and α-amino acids, have successfully introduced to produce pyrrolidine rings with solubilizing triethylene glycol chains or octyl groups [6,7]. Functionalized SWNTs showed one pyrrolidine ring correspond to about 95 carbon atoms of the SWNT and solubility values closer to 50 mg mL^{-1} in chloroform. 1,3-DC of nitrile imines and nitrile oxides has been carried out to attach 2,5-diarylpyrazoline or pyridyl-isoxazoline rings, respectively on nanotube surface [16,17]. Microwave induced functionalization of carbon nanotubes has also been described showing that 1,3-DC of nitrile imines to SWNT sidewall under microwave conditions was faster than conventional heating [18]. Brunetti et al. reported the microwave-assisted rapid cycloaddition to pristine nanotubes in solvent free conditions using octyl substituted aziridines [19]. Modified SWNTs displayed ~1 functional group for every 51 SWNT carbon atom and they were slightly soluble in DMF (0.13 mg mL^{-1}) and dichloromethane (0.11 mg mL^{-1}). It was shown that the microwave assisted cycloaddition of aziridines were much more efficient than the classical thermal conditions for azomethine ylides [6].

In our research group, it has been demonstrated that SWNTs can undergo 1,3-DC with azomethine imines, 3-phenyl-phthalazinium-1-olate, to yield a bridged phenyl phthalazine groups with coordination sites for various metals including Cu, Co, and Pt [4]. We have also shown that pyridinium ylides generated from simple Kröhnke salts undergo a 1,3-DC to SWNTs to afford indolizine functionalized fluorescent SWNTs [5]. Reaction was believed to occur with the pyridinium ylide first adding to the nanotube surface to form a pyrrolidine ring, closely followed by the addition of a second ylide to the addendum on the nanotube surface to afford an indolizine. The mechanism of pyridinium ylide cycloaddition was attributed to electron transfer from the SWNT to the 1,3-dipole assuming similar selective addition of diazonium salt to SWNTs, which is in agreement with metallic SWNTs, which have a finite DOS at the Fermi level, being more reactive than semiconducting SWNTs [20]. However, it is believed that reactivity/mechanism/regioselectivity of pyridinium ylide cycloaddition to SWNTs might be different from diazonium salt addition to SWNTs since it is well studied that HOMO–LUMO energy levels of both dipole (pyridinium ylide) and dipolarophile (C=C bond on CNT surface) participate a significant role during cycloaddition reactions [21].

In this paper, the reactivity/mechanism of pyridinium ylide addition to SWNTs is therefore assessed theoretically using semi-empirical PM3 (RHT) calculations. The regioselectivity of the second ylide addition (as addendum) to pyridine ring to afford an indolizine is also discussed theoretically. 1,3-DC of two new pyridinium ylides, readily prepared from simple Kröhnke salts *N*-(4-methyl sodium benzenesulfonate)-pyridinium bromide and *N*-(4-nitrobenzyl)-pyridinium bromide, is presented. Structural assignment of Kröhnke salts is carried out by NMR and FTIR. Covalent addition to SWNT surface is probed via UV–vis–NIR, FTIR, TGA–MS, XPS and resonance Raman spectroscopy.

2. Material and methods

2.1. Computational method

All computational work to have the optimized, well-defined structures of SWNTs and ylides and exploration of their reactivity were held by using HyperChem 7.0 package program using semi-empirical PM3 (RHT) calculations [22]. As a minimization algorithm throughout the calculations, a conjugate gradient, Polak–Ribiere (convergence limit of 0.0001 kcal mol^{-1}) and the RMS gradient condition of 0.0001 kcal (Å mol)$^{-1}$ were chosen.

2.2. Preparation of purified SWNTs

Purified SWNTs produced by the HiPco method and supplied by Unidym, USA, were further purified by heating in air at 400 °C, then soaking in 6 M HCl overnight, followed by filtration over a polycarbonate membrane (0.2 μm), and washing with de-ionized water until neutral pH was reached [23]. The purified SWNTs were annealed under vacuum (10^{-2} mbar) at 900 °C to remove residual carboxylic acid functional groups and any adsorbed gases or solvents.

2.3. SWNT–indolizine (SWNT2)

SWNTs (10 mg) were dispersed in *N*,*N*-dimethylformamide (DMF) (15 mL) using mild sonication in an ultrasonic bath (Ultrawave U50, 30–40 kHz) for 5 min. The pyridinium salt (1) (1.468 g, 4.17 mmol) and triethylamine (0.58 mL, 4.177 mmol) was then added to the dispersion. The reaction mixture was then heated to 150 °C at 2 bar pressure, in a heat and pressure resistant vessel, with microwaves for 1 h (150 W for 5 min followed by 20 W for 50 min at 2.54 GHz) using a Biotage Initiator Sixty which resulted in the formation of SWNT2 following the pyrrolidine attached SWNT intermediate (SWNT1) formation. The functionalized SWNTs were collected via filtration through a PTFE membrane (0.2 μm). The solid SWNTs were then transferred to a cellulose thimble, and impurities and unreacted reagents were removed by Soxhlet extraction using acetonitrile for 18 h. The SWNTs were then dispersed in de-ionized water (50 mL) and filtered through a PTFE membrane (0.2 μm), dispersed in acetone (50 mL) and filtered through a PTFE membrane (0.2 μm), and finally dispersed in ethanol (50 mL) and filtered through a PTFE membrane (0.2 μm) and dried overnight at 120 °C to afford SWNT–indolizine (SWNT2).

2.4. SWNT–indolizine (SWNT4)

SWNT4 was synthesized as described above following the formation of SWNT3 intermediate using 10 mg of SWNTs, pyridinium salt (2) (1.230 g, 4.17 mmol) and triethylamine (0.58 mL, 4.177 mmol).

2.5. Characterization

^{1}H NMR and ^{13}C NMR spectra were recorded on Bruker Avance-400 spectrometer operating at (^{1}H) 400.13 MHz and (^{13}C) 100.62 MHz. Chemical shifts are reported in ppm. Infrared spectra

of pure compounds (powder) were recorded using a Perkin–Elmer Spectrum 100 equipped with a Pike ATR fitted with a Ge crystal. XPS studies were performed at NCESS, Daresbury Laboratory, using a Scienta ESCA 300 hemispherical analyzer with a base pressure under 3×10^{-9} mbar. The analysis chamber was equipped with a monochromated $Al_{K\alpha}$ X-ray source ($h\nu = 1486.6$ eV). Charge compensation was achieved (if required) by supplying low-energy (<3 eV) electrons to the samples. XPS data were referenced with respect to the corresponding C 1s binding energy of 284.5 eV, which is typical for carbon nanotubes [4]. Photoelectrons were collected at a 45° takeoff angle, and the analyzer pass energy was set to 150 eV, giving an overall energy resolution of 0.4 eV. Elemental compositions were determined using the XPS survey spectra as described in literature [24]. TGA–MS data were recorded on 1–3 mg of sample using a Perkin–Elmer Pyris I thermogravimetric analyzer coupled to a Hiden HPR20 mass spectrometer. Data were recorded in flowing He (20 mL min^{-1}) at a ramp rate of 10 °C min^{-1} to 900 °C after being held at 120 °C for 30 min to remove any residual solvent. UV/Vis–NIR absorption spectra were recorded on a Perkin–Elmer Lambda 900 spectrometer. The samples were prepared by dispersing the nanotube material in DMF by sonication in an ultrasonic bath (Ultrawave U50, 30–40 kHz) for 5 min followed by filtration through a plug of cotton wool to remove particulates after allowing the solution to stand for 2 h. Raman spectra were recorded using a Jobin Yvon Horiba LabRAM spectrometer in a back scattered confocal configuration using Nd:YAG (532 nm, 2.33 eV) laser excitation. All spectra were recorded on solid samples over several regions and were referenced to the silicon line at 520 cm^{-1}.

3. Results and discussions

3.1. Theoretical assessment of 1,3-DC of pyridinium ylides to (8,8) SWNT

Purified HiPco–SWNTs (diameter ~0.8–1.2 nm) were used in experiments, and theoretical calculations were therefore performed using short and metallic (8,8) SWNT segments as nanotube models (predicted diameter ~1.1 nm). The general theory for perturbation of the frontier molecular orbital was applied to assess the reactivity/mechanism/regioselectivity of pyridinium ylides (ylide1 and ylide2) cycloaddition to (8,8) SWNT, Fig. 1.

N-(Ethoxycarbonylmethyl)-pyridinium ylide, [5] previously used for the preparation of indolizine modified fluorescent SWNTs, was used as a reference ylide structure ($ylide_{Ref}$) for comparison, Fig. 1. HOMO–LUMO energies of corresponding ylides and (8,8) SWNT segments were estimated via semi-empirical PM3 method at the level of restricted Hartree–Fock (RHF) approach [25]. The effect of nanotube length on HOMO–LUMO band gap was studied using 20 different (8,8) SWNT segments, systematically starting from the smallest (10.87 Å diameter/2.41 Å length) to the longest (~11 Å diameter/50–10000 Å length) (8,8) SWNT segment, Table 1.

Table 1
HOMO–LUMO orbital energy levels and HOMO–LUMO energy gap of (8,8) SWNT segments.

(8,8) SWNT segment/[a]/[b]	HOMO/eV	LUMO/eV	HOMO–LUMO gap/eV
Segment 1/10.87/2.41	−7.95	−1.27	6.68
Segment 2/10.97/4.90	−7.34	−2.18	5.16
Segment 3/10.99/9.79	−7.06	−2.69	4.37
Segment 4/10.94/12.27	−6.90	−3.01	3.89
Segment 5/10.98/17.17	−6.80	−3.24	3.56
Segment 6/11.08/19.65	−6.74	−3.40	3.34
Segment 7/10.91/24.56	−6.70	−3.52	3.18
Segment 8/11.17/27.05	−6.67	−3.62	3.05
Segment 9/11.05/31.93	−6.65	−3.70	2.95
Segment 10/11.04/34.41	−6.64	−3.76	2.88
Segment 11/11.03/39.30	−6.63	−3.82	2.81
Segment 20≥/~11/50–10,000	−6.60	−3.96	2.64

[a] Diameter of SWNT segment in Å.
[b] Length of SWNT segment Å.

Consistent with the previously reported HOMO–LUMO energy gap estimations of (5,5) [26] and (6,6) [27] SWNTs HOMO–LUMO energy gap of (8,8) SWNT decreased when SWNT length increased. This trend was not surprising since HOMO–LUMO gaps of metallic SWNTs with respect to tube length is expected to converge to zero at finite length [15,27]. Herein reactivity assessment of pyridinium ylides to SWNTs was made using $SWNT_{segment\ 10}$ with HOMO and LUMO energies of −6.64 and −3.76 eV, respectively. HOMO–LUMO energies of ylide1, ylide2 and corresponding $ylide_{Ref}$ [5] were also estimated using the same approach, and results were compared with $SWNT_{segment\ 10}$ in Fig. 2.

Extensive work has been devoted to understand the reactivity/mechanism of cycloaddition reactions. Among the types of 1,3-DCs [28–31], similar to that of azomethine ylides to electron deficient dipolarophiles [21], 1,3-DCs of pyridinium ylides to SWNTs are expected to be $HOMO_{dipole}$–$LUMO_{dipolarophile}$ controlled (Type I). Substituent effect ($-SO_3^-Na^+$ and $-NO_2$) on reactivity of 1,3-DC

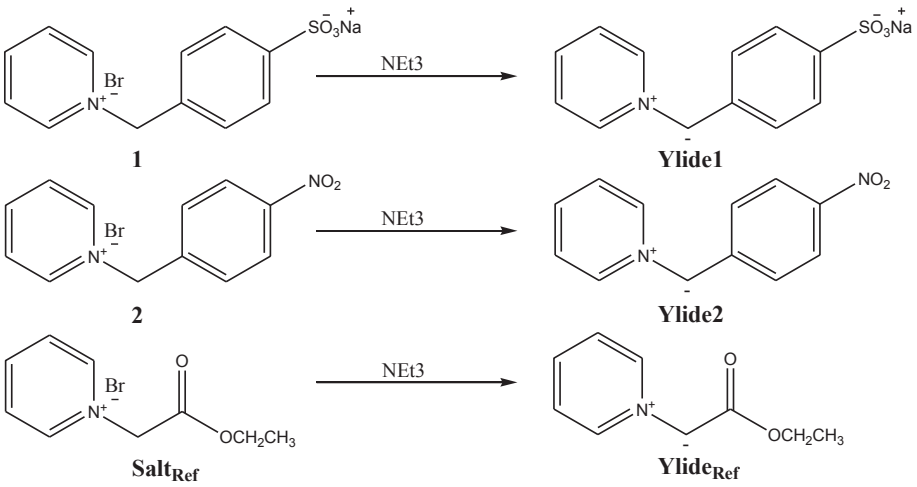

Fig. 1. Schematic representation for preparation of pyridinium ylides by the addition of base (NEt_3) to pyridinium bromide salts.

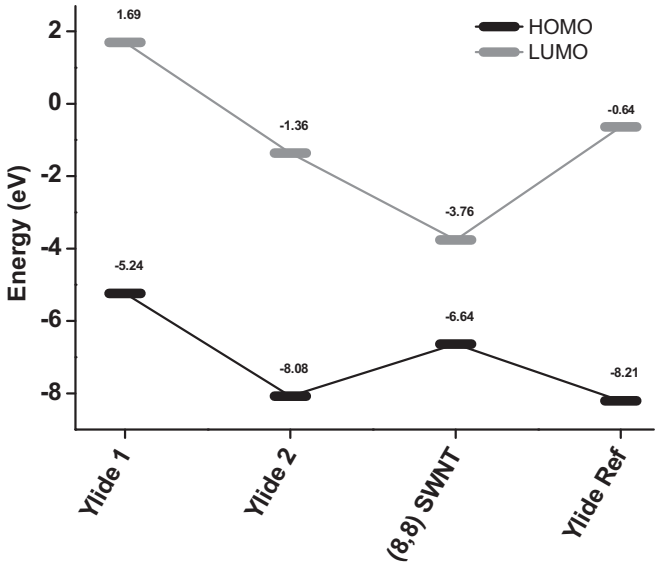

Fig. 2. HOMO/LUMO energy levels of ylide1, ylide2, $ylide_{Ref}$ and (8,8) SWNT for HOMO–LUMO gap comparison.

might be understood in terms of the orbital symmetry and FMO theory [32]. FMO energy predictions of pyridinium ylides and (8,8) SWNT (Fig. 2) displays that $HOMO_{ylide}$–$LUMO_{(8,8)\ SWNT}$ energy gap (1.48, 4.32 and 4.45 eV for $HOMO_{ylide1}$–$LUMO_{(8,8)\ SWNT}$, $HOMO_{ylide2}$–$LUMO_{(8,8)\ SWNT}$ and $HOMO^{Ref}_{ylide}$–$LUMO_{(8,8)\ SWNT}$, respectively) is smaller than that of $LUMO_{ylide}$–$HOMO_{(8,8)\ SWNT}$ energy gap (8.33, 5.28 and 6.00 eV for $LUMO_{ylide1}$–$HOMO_{(8,8)\ SWNT}$, $LUMO_{ylide2}$–$HOMO_{(8,8)\ SWNT}$ and $LUMO^{Ref}_{ylide}$–$HOMO_{(8,8)\ SWNT}$, respectively). In contrast to diazonium salt addition [20] to SWNTs where reaction follows a radical mechanism with electron transfer from SWNTs to diazonium salt, FMO calculations of pyridinium ylides and SWNTs suggest a $HOMO_{ylide}$–$LUMO_{(8,8)\ SWNT}$ controlled 1,3-DC where the charges are probably transferred from $HOMO_{ylides}$ to $LUMO_{(8,8)\ SWNTs}$. Furthermore the $HOMO_{ylide1}$–$LUMO_{(8,8)\ SWNT}$ energy gap (1.48 eV) is predicted as the smallest compared to $HOMO_{ylide2}$–$LUMO_{(8,8)\ SWNT}$ and $HOMO^{Ref}_{ylide}$–$LUMO_{(8,8)\ SWNT}$ energy gap with 4.32 and 4.45 eV, respectively. It is therefore theoretically expected that the reactivity of ylide1 should be higher than that of ylide2 and $ylide_{Ref}$ which are similar in reactivity.

In cycloaddition reactions, regioselectivity has gained particular interest since possible dipole/dipolarophile orientations due to the differences in atomic orbital energies might yield cycloadducts having different geometries. Herein, regioselectivity of the second pyridinium ylide addition as addendum to pyrrolidine attached on SWNT surface was studied by estimating the coefficients for the atomic orbital of both free pyridinium ylides (ylide1, ylide2 and $ylide_{Ref}$) and pyrrolidine attached on SWNT (SWNT1 and SWNT3 in Fig. 4). Calculations were performed using both SWNT segment 3 and segment 6. However, PM3 calculations of pyrrolidine attached SWNT from segment 3, segment 6 and $ylide_{Ref}$ yielded inexplicable negative (and nearly equal to zero) HOMO–LUMO energy coefficients on the C2 and C3, probably due to pyrrolidine moiety appeared as being so small compared to the rest of the SWNT structure (See ESI Figs. S1 and S2 for the energy values of pyrrolidine attached SWNT from segment 3). In order for discussing the probability of second 1,3-DCs as addendum to pyrrolidine attached on SWNT surface, a pyrrolidine attached pyrene structure was therefore chosen as a simple molecular model of pyrrolidine attached on SWNT surface. For the assumptions of the second 1,3-DCs of SWNTs with ylides, FMO energy predictions were further performed on pyrrolidine modified pyrene structure and, HOMO–LUMO energy coefficients for the atomic orbital of ylide1, ylide2 and $ylide_{Ref}$ and their corresponding pyrene adducts ($ylide1_{pyrene}$, $ylide2_{pyrene}$ and $ylide_{Ref\text{-}pyrene}$) were tabulated in Table 2.

HOMO–LUMO energy band gaps between ylides and their pyrene adducts propose that the 1,3-DC of second pyridinium ylides to $ylide_{pyrene}$ adducts are $HOMO_{ylide}$–$LUMO_{ylide-pyrene}$ controlled since the energy band gap is smaller than $HOMO_{ylide-pyrene}$–$LUMO_{ylide}$. Regioselectivity of second cycloaddition was predicted using the atomic orbital coefficients corresponding to $HOMO_{ylide}$–$LUMO_{ylide-pyrene}$. According to Fukui [33], reactions can be favorable in the direction of maximal HOMO–LUMO overlapping of larger coefficients at the reactive sites. The most favorable interactions between corresponding ylides and $ylide_{pyrene}$ adducts to form the most favorable regioisomer conformation are given in Fig. 3. Second ylide addition to $ylide_{pyrene}$ structure is therefore anticipated to proceed via $ylide_{C2/C6}$–$ylide_{pyrene\text{-}C3}$ and $ylide_{C7}$–$ylide_{pyrene/C2}$ interactions to produce the same regioisomer conformations. Considering the theoretical calculations performed for pyrrolidine attached pyrene structure, it is also expected that formation of the same type of regioisomers are favorable for SWNTs after the 1,3-DC of pyridinium ylides, Fig. 3.

3.2. Synthesis and characterization of indolizine modified SWNTs

Purified SWNTs were reacted under microwave conditions with pyridinium ylides generated *in-situ* via the addition of triethylamine (NEt_3) to the Kröhnke salts *N*-(4-methyl sodium benzene sulfonate)-pyridinium bromide (1) and *N*-(4-nitrobenzyl)-pyridinium bromide (2) to afford SWNT with indolizine groups covalently bound to the nanotube surface, SWNT2 and SWNT4, Fig. 4. Kröhnke salts (1) and (2) were easily prepared using a modified literature procedure [5] by the addition of sodium 4-(bromomethyl)benzenesulfonate [34] and 4-nitrobenzylbromide, respectively, to pyridine at room temperature (see Fig. 1). The resulting crude salts were washed with acetone/ethanol to remove excess pyridine, sodium 4-(bromomethyl) benzenesulfonic acid and 4-nitrobenzylbromide to afford the pyridinium bromide salts (1) (88%) and (2) (90%). Isolated salts (1 and 2) were characterized using FTIR, ^1H and ^{13}C NMR. Ylides produced via the addition of NEt_3 to the corresponding pyridinium bromide salts (1 and 2) could not be isolated due to the unstable nature of the pyridinium ylides and all reactions were carried out *in-situ*.

FTIR spectra of purified SWNTs and the indolizine-functionalized SWNTs (SWNT2 and SWNT4) are presented in Fig. 5. Consistent with the previous literature purified SWNT material demonstrates expected IR frequencies at *ca.* 2916, 1700, 1236 and 1055 cm^{-1} [5]. FTIR spectrum of SWNT2 displays the characteristic SO_2 symmetric stretching ($\nu_{(SO)}$ 1150 cm^{-1}) and SO_2 asymmetric stretching ($\nu_{(SO)}$ 1338 cm^{-1}) as an indication of sulfonate

Table 2
HOMO–LUMO orbital energy (*E*/eV) of ylide1, ylide2 and $ylide_{Ref}$ and their pyrene adducts and atomic orbital coefficients (*C*/eV).

Ylide		*E*/eV	*C*2/eV	*C*3/eV	*C*6/eV	*C*7/eV
ylide1	HOMO	−5.24	0.37	–	0.37	−0.50
	LUMO	1.69	−0.08	–	−0.28	−0.43
$ylide1_{pyrene}$	HOMO	−5.99	0.18	0.23	–	–
	LUMO	0.87	−0.02	0.02	–	–
ylide2	HOMO	−8.08	0.36	–	0.34	−0.61
	LUMO	−1.36	−0.024	–	−0.24	−0.19
$ylide2_{pyrene}$	HOMO	−8.62	−0.61	−0.07	–	–
	LUMO	−1.14	0.01	−0.01	–	–
$ylide_{Ref}$	HOMO	−8.22	−0.38	–	−0.38	0.69
	LUMO	−0.64	0.13	–	0.36	0.35
$ylide_{Ref-pyrene}$	HOMO	−8.31	0.21	0.18	–	–
	LUMO	−0.93	0.02	−0.01	–	–

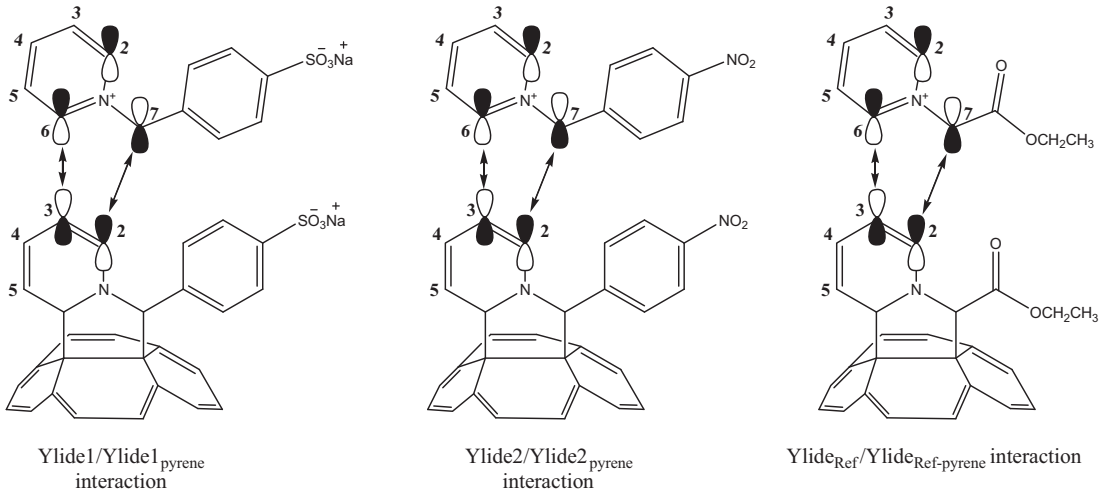

Fig. 3. Interactions between corresponding ylides and ylide$_{pyrene}$ adducts to form the most favorable regioisomer conformation.

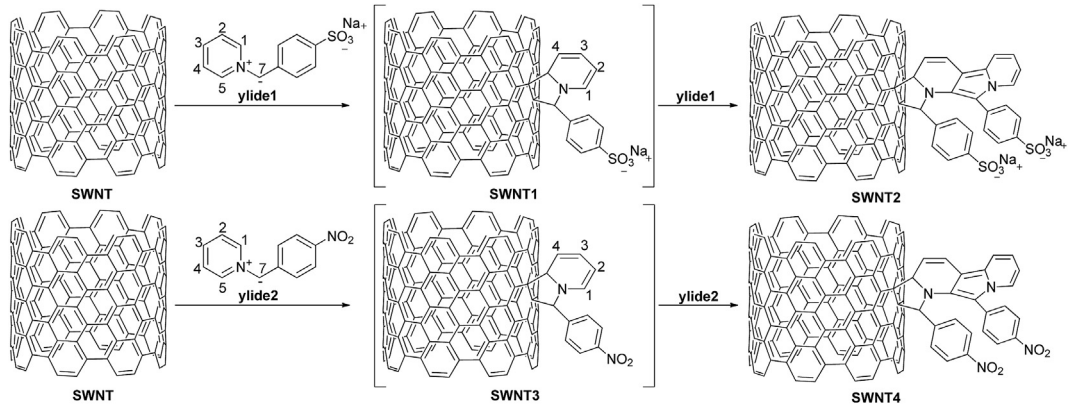

Fig. 4. Schematic representation of the 1,3-dipolar cycloaddition of a pyridinium ylide, generated by the action of base on the Kröhnke salt (1) and (2) to the sidewalls of the SWNTs to form an indolizine (SWNT2) and (SWNT4).

group [35]. The band at 1520 cm^{-1} in FTIR spectrum of SWNT4 is attributed to NO_2 asymmetric stretching ($\nu_{(NO)}$ 1520 cm^{-1}), confirming the availability of nitro groups [35]. Two bands at *ca.* 1580 and 1400 cm^{-1} in both spectra of SWNT2 and SWNT4 are assigned to characteristic stretching of indolizine [36].

Raman spectroscopy of SWNTs has widely been studied to identify covalent surface modification. The disorder band or D-band at about 1300 cm^{-1} is related to the reduction in symmetry of the SWNTs, and the change in intensity/area of which provides the information of covalent surface modification when compared to that of the tangential band (G-band) at about 1590 cm^{-1} [9,37]. Thus direct evidence for the covalent addition of pyridinium ylides (ylide1 and ylide2) to SWNTs can be provided by Raman spectroscopy. Raman spectra of SWNT2 and SWNT4 (excited at 532 nm and normalized to the G-band intensity) display slightly enhanced D-band at *ca.* 1350 cm^{-1} compared to unmodified purified SWNTs ($A_D/A_G = 0.061 \pm 0.001$), with an A_D/A_G ratio of 0.194 ± 0.005 and 0.14 ± 0.004, respectively, indicative of groups covalently attached to the surface of the nanotubes, Fig. 6 [4,5,9,37,38]. 1,3-DC of ylide1 and ylide2 are found to be selective to large diameter SWNTs. Raman spectra of modified SWNTs excited at 632.8 nm and normalized to G-band further reveal that ylide1 is more selective to large diameter SWNTs than ylide2, displaying more suppressed RBMs related to large diameter SWNTs at ~187, 197, 209 cm^{-1} for SWNT2 compared to RBMs of SWNT4 (See ESI Fig. S3).

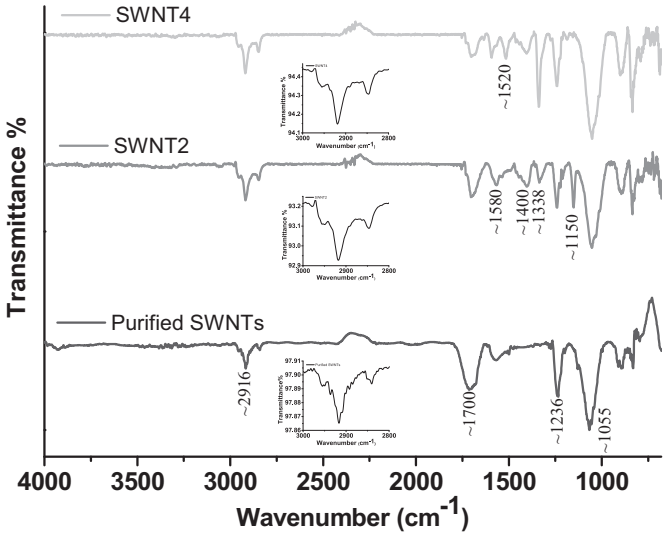

Fig. 5. Normalized and offset FTIR spectra of purified SWNTs, indolizine functionalized SWNTs (SWNT2) prepared by *N*-(4-methyl sodium benzenesulfonate)-pyridinium bromide and indolizine functionalised SWNTs (SWNT4) prepared by *N*-(4-nitrobenzyl)-pyridinium bromide (inset: a little segment (3000–2800 cm^{-1}) indicating the % scale for each of the spectra).

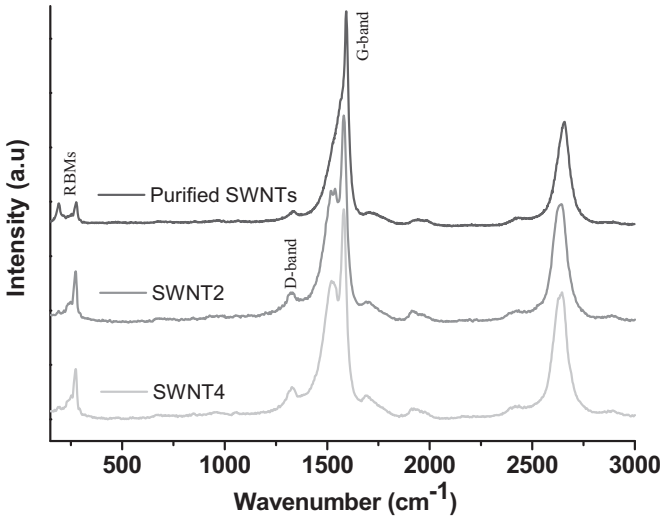

Fig. 6. Normalized and offset Raman (532 nm, 2.33 eV) spectra of purified SWNTs, indolizine functionalized SWNTs (SWNT2) prepared by *N*-(4-methyl sodium benzenesulfonate)-pyridinium bromide and indolizine functionalised SWNTs (SWNT4) prepared by *N*-(4-nitrobenzyl)-pyridinium bromide.

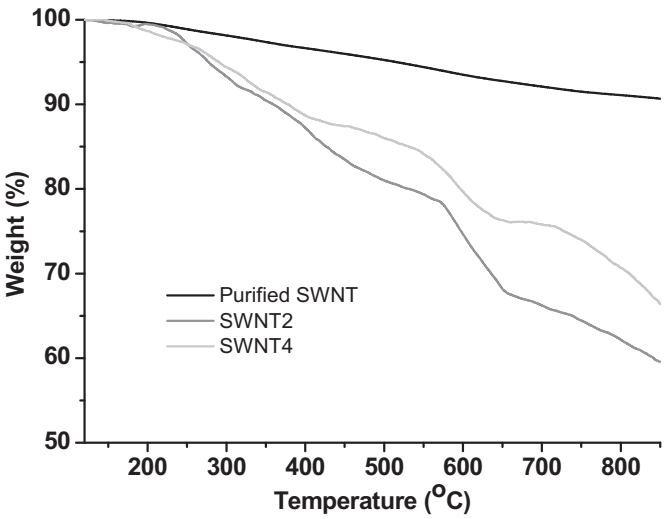

Fig. 8. TGA–MS data (10 °C min^{-1}) of purified SWNTs, SWNT2 prepared by *N*-(4-methyl sodium benzenesulfonate)-pyridinium bromide and SWNT4 prepared by *N*-(4-nitrobenzyl)-pyridinium bromide.

It is well studied that the electronic properties of CNTs are disrupted via covalently introducing sp^3-hybridized carbon atoms to the surface. Any suppression in the characteristic absorption bands corresponding to the electronic transitions between van Hove singularities is attributed to covalent functionalization. However, such a decrease is highly dependent on the concentration of the covalently attached surface groups. Small decreases in the intensity of transition bands are ascribed to non-destructive/light surface functionalization where the electronic properties of CNTs are likely to be conserved. Changes in the electronic properties of nanotubes can be probed best via electronic spectroscopy in the solution phase. The UV–vis–NIR spectra of SWNT2 and SWNT4, Fig. 7, show the suppression of the bands in the region 400–1400 nm, present due to the van Hove singularities, indicating that pyridinium ylide addition to SWNTs is non-destructive [37,39].

From Beer's law, using an extinction coefficient of 30 mL mg^{-1} cm^{-1} and absorption values at $\lambda = 700$ nm [40], concentration of a stable dispersion of SWNT2 and SWNT4 in DMF was estimated 23 and 20 μg mL^{-1} respectively, compared to 3 μg mL^{-1} for as-received purified SWNTs.

Quantification of the covalently attached surface groups was carried out by thermogravimetric analysis (TGA) coupled with mass spectrometry (MS). TGA–MS of SWNT2 and SWNT4 shows a weight loss of approximately 24 and 34% respectively, at 700 °C compared to *ca.* 8% for purified SWNTs, Fig. 8. This corresponds to the presence of approximately 1 functional group for ~200 (~0.96 N%) and ~101 (~1.98 N%) carbon atoms respectively. As expected from HOMO–LUMO energy levels, reactivity of ylide2 is in close agreement with $ylide_{Ref}$. In contrast, ylide1 shows surprisingly less reactivity towards SWNTs although HOMO–LUMO energy band gap is smaller than ylide2. It is thought that decrease in reactivity of ylide1 is due to the ionic character of electron withdrawing sodium sulfonate ($-SO_3^-Na^+$) salt which probably destabilizes *in-situ* produced 1,3-dipole (ylide1) even though it decreases HOMO–LUMO gap of ylide1.

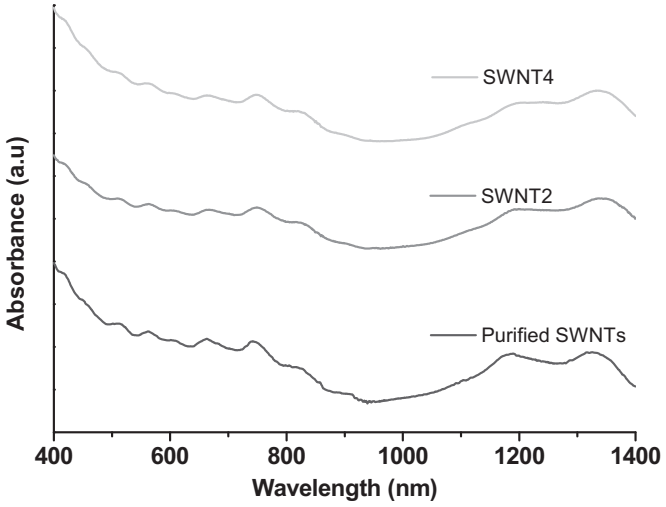

Fig. 7. Normalized (at 400 nm) and offset UV–vis–NIR spectra, recorded in DMF, of purified SWNTs, SWNT2 prepared by *N*-(4-methyl sodium benzenesulfonate)-pyridinium bromide and SWNT4 prepared by *N*-(4-nitrobenzyl)-pyridinium bromide.

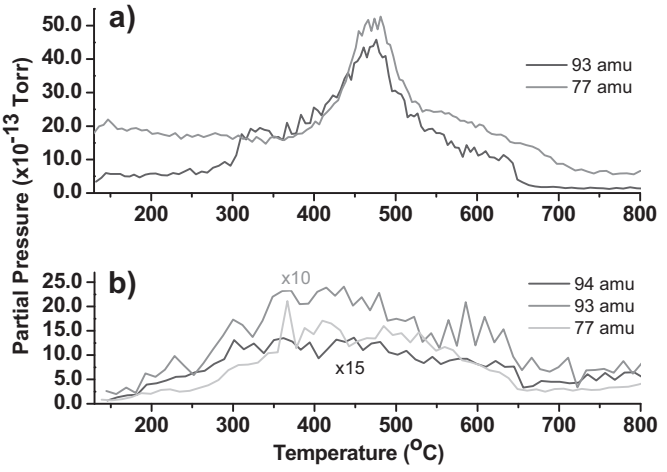

Fig. 9. a) MS trace of *N*-methylpyridinium (94 amu) and phenyl fragment (C_6H_5, 77 amu) given off during heating of SWNT2. b) MS trace of *N*-methylpyridinium (94 amu), phenoxy fragment (C_6H_5O, 93 amu) and phenyl fragment (C_6H_5, 77 amu) given off during heating of SWNT4.

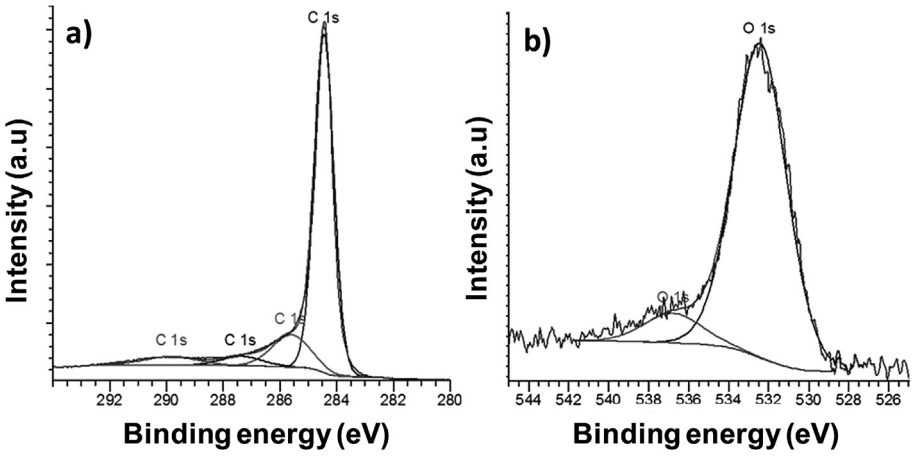

Fig. 10. a) C 1s XPS spectrum of the purified SWNTs and the position of components b) O 1s XPS spectrum of the purified SWNTs and the position of components.

Mass spectrometry results corroborate TGA data and display the peak of mass loss between 200 and 700 °C for the indolizine modified SWNTs (SWNT2 and SWNT4), Fig. 9. However it was not possible to observe the parent ion of the indolizine due to its high molecular mass. Although the parent ion of the indolizine was not observed, fragments relating to the *N*-methylenepyridinium (93 amu) and phenyl (77 amu) for SWNT2 and, *N*-methylpyridinium (94 amu), phenoxy (C_6H_5O, 93 amu) and phenyl (C_6H_5, 77 amu) for SWNT4 were detected by mass spectrometry.

3.3. XPS analysis of indolizine modified SWNTs

XPS is used as an informative surface chemical analysis technique that provides a wealth of information related to elemental composition, empirical formula, chemical state and electronic state of the elements present in sample. Thus XPS has been extensively employed to monitor the surface chemistry of functionalised SWNTs [3–5,41,42]. It has generally been used to identify the heteroatom elements (F, I, N and S) and to quantify degree of

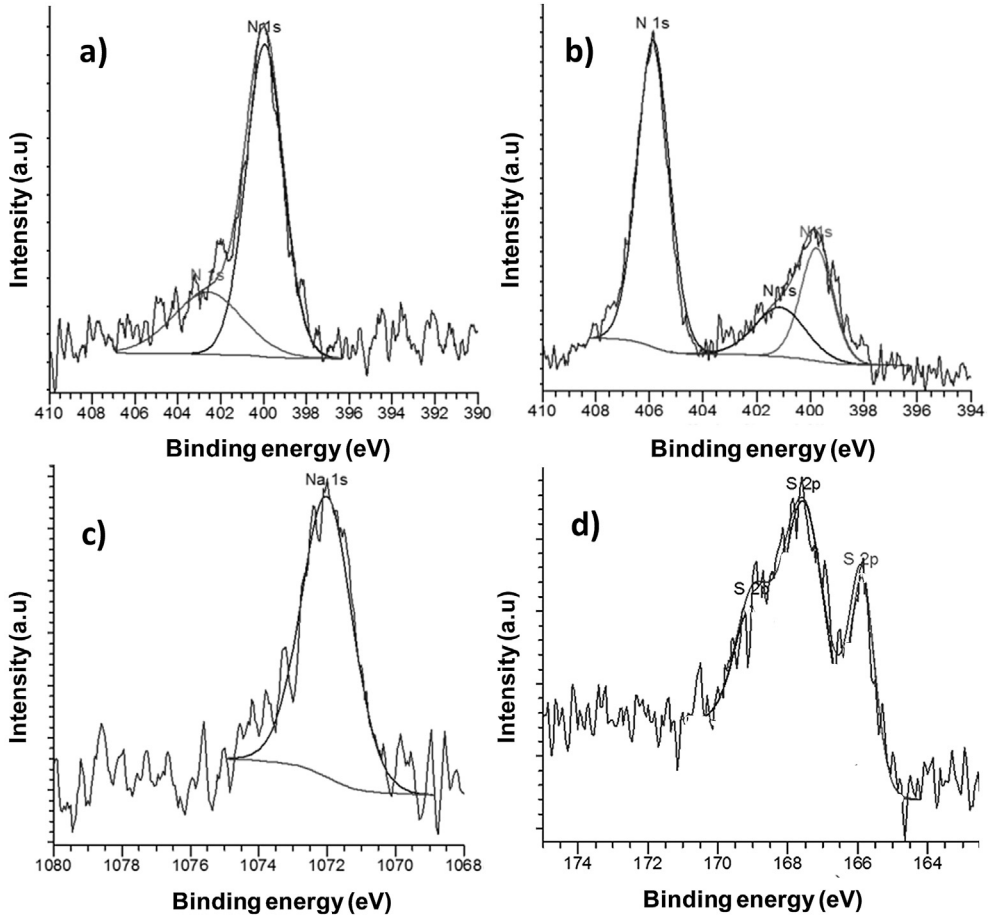

Fig. 11. a) N 1s XPS spectrum of SWNT2 and the position of components; b) N 1s XPS spectrum of SWNT4 and the position of components; c) Na 1s XPS spectrum of SWNT2 with single peak *ca.* 1072 eV; d) S 2p XPS spectrum of SWNT2 with three peaks *ca.* 165.83, 167.53 and 169.03 eV.

modification. However, quantification can be complicated by overlapped binding energies. Therefore the de-convolution of XPS bands in a spectrum is essential to study fine structures of SWNTs.

XPS survey analysis of purified SWNTs shows presence of 95.55 ± 0.41% C and 4.45 ± 0.24% O atoms. Analysis of de-convoluted C 1s XPS spectrum of purified SWNTs, Fig. 10, shows four components having binding energies at 284.4, 285.4, 287.2 and 289.8 eV attributable to graphitic carbon (−C*═C*−) (π-conjugated carbon system and/or unsaturated aliphatic rests) [43,44], tetrahedrally bonded carbon (C−H and C−C) [45], carbonyl (or ether) [46] and carboxyl group (−O−C*═O) [44,47], respectively. O 1s XPS spectrum consists of two main components at 532.4 and 536.7 eV corresponded to carboxyl (−O−C═O*) [44] and hydroxyl (−C−O*H) [48], respectively. The presence of O atom in purified SWNT sample can be due to either physisorbed water and/or carbon dioxide contamination [49], or the oxidized SWNTs produced during SWNT purification [43]. C 1s XPS spectra of indolizine modified SWNTs (SWNT2 and SWNT4) demonstrate similar features compared to C 1s XPS spectrum of unmodified purified SWNTs. (See ESI Figs. S4 and S5) However, the de-convolution of O 1s spectra of SWNT2 and SWNT4 illustrates a broadened line shape with a new shoulder positioned at *ca.* 531 eV, attributable to the introduction of oxygen containing groups (*e.g.* NO_2 and SO_3) to nanotube surface when compared to O 1s XPS spectrum of purified SWNTs [4]. N 1s XPS spectra of SWNT2 and SWNT4 display two main components positioned at *ca.* 399.8 and 401.7 eV, Fig. 11.

N 1s component at 399.8 eV is characteristic of sp^2 hybridized pyridine nitrogen and the component at 401.7 eV is attributed to quaternary pyridine [50–52]. As expected an additional strong peak corresponding to $-NO_2$ group is also observed at *ca.* 405.8 eV in N 1s XPS spectrum of SWNT4 [53]. XPS spectrum of SWNT2 also displays characteristic S 2p peaks *ca.* 165.8, 167.5 and 169.0 eV confirming the presence of sulfur and Na 1s at 1072 eV in the modified material. The number of S 2p peaks clearly suggests the presence of more than one sulfur environment. The reason of this could be the degradation of sulfonate ($-SO_3^-Na^+$) groups under microwave conditions. However, it is not clear from the unresolved S 2p XPS spectrum which of the sulfonic species is available in the material, Fig. 11 [45,54,55]. Elemental composition analysis of nitrogen in SWNT2 and SWNT4 shows the presence of 1.48 ± 0.41 and 2.09 ± 0.29 atomic percent (at.%) nitrogen, respectively, and they are in close agreement with the values determined by TGA.

4. Conclusion

The frontier molecular orbital energies (HOMO and LUMO) indicate that 1,3-DC reaction of pyridinium ylides to (8,8) SWNT probably occurs via electron transfer from ylide to (8,8) SWNT and, reaction is therefore expected to be $HOMO_{ylide}$−$LUMO_{(8,8)\ SWNT}$ controlled cycloaddition (Type I). Substituent effect studies suggest that the reactivity of pyridinium ylide might be manipulated taking the advantage of strong electron-withdrawing (EW) substituents on phenyl ring. In the present study it is experimentally observed that ionic character of EW substituent ($-SO_3^-Na^+$) decreases the reactivity of pyridinium ylide although it decreases HOMO−LUMO energy gap. It is likely to generate fluorescent SWCNTs by reducing groups attached to indolizine ring. Ylides with smaller HOMO−LUMO gap is found to be more selective to large diameter SWNTs implying the possibility to make use of the 1,3-DC of substituted pyridinium ylides with chemistry to sort SWNTs diameter-specifically. Furthermore the use of strong EW groups might also pave the way for surface modification of graphene although it has been theoretically reported that covalent addition of azomethine ylides to graphene surface are not favorable [56].

Acknowledgments

We thank Dr. Graham Beamson of the National Centre for Electron Spectroscopy and Surface Analysis (NCESS) at Daresbury Laboratory for technical assistance and useful discussions on the XPS measurements, Doug Carswell for recording the TGA data, and the EPSRC (EP/E025722/1). M.K.B. thanks the Scientific and Technological Research Council of Turkey (TÜBİTAK).

Appendix A. Supplementary data

Supplementary data related to this article can be found at http://dx.doi.org/10.1016/j.matchemphys.2014.01.045.

References

[1] R.H. Baughman, A.A. Zakhidov, W.A. de Heer, Science 297 (2002) 787–792.
[2] Y.P. Sun, K.F. Fu, Y. Lin, W.J. Huang, Acc. Chem. Res. 35 (2002) 1096–1104.
[3] M.K. Bayazit, L.S. Clarke, K.S. Coleman, N. Clarke, J. Am. Chem. Soc. 132 (2010) 15814–15819.
[4] M.K. Bayazit, K.S. Coleman, Chem. Asian J. 7 (2012) 2925–2930.
[5] M.K. Bayazit, K.S. Coleman, J. Am. Chem. Soc. 131 (2009) 10670–10676.
[6] V. Georgakilas, K. Kordatos, M. Prato, D.M. Guldi, M. Holzinger, A. Hirsch, J. Am. Chem. Soc. 124 (2002) 760–761.
[7] N. Tagmatarchis, M. Prato, J. Mater. Chem. 14 (2004) 437–439.
[8] M.K. Bayazit, A. Suri, K.S. Coleman, Carbon 48 (2010) 3412–3419.
[9] S.A. Hodge, M.K. Bayazit, K.S. Coleman, M.S.P. Shaffer, Chem. Soc. Rev. 41 (2012) 4409–4429.
[10] I. Kumar, S. Rana, J.W. Cho, Chem. Eur. J. 17 (2011) 11092–11101.
[11] V. Georgakilas, A.B. Bourlinos, R. Zboril, T.A. Steriotis, P. Dallas, A.K. Stubos, C. Trapalis, Chem. Commun. 46 (2011) 1766–1768.
[12] X. Wu, H. Cao, B. Li, G. Yin, Nanotechnology 22 (2011).
[13] X. Lu, F. Tian, X. Xu, N.Q. Wang, Q. Zhang, J. Am. Chem. Soc. 125 (2003) 10459–10464.
[14] S. Dresselhaus, G. Dresselhaus, P. Avouris, Carbon Nanotubes: Synthesis, Structure, Properties, and Applications, Springer, 2001.
[15] E. Joselevich, ChemPhysChem 5 (2004) 619–624.
[16] M. Alvaro, P. Atienzar, P. la Cruz, J.L. Delgado, V. Troiani, H. Garcia, F. Langa, A. Palkar, L. Echegoyen, J. Am. Chem. Soc. 128 (2006) 6626–6635.
[17] M. Alvaro, P. Atienzar, P. de la Cruz, J.L. Delgado, H. Garcia, F. Langa, J. Phys. Chem. B 108 (2004) 12691–12697.
[18] Y.B. Wang, Z. Iqbal, S. Mitra, Carbon 43 (2005) 1015–1020.
[19] F.G. Brunetti, M.A. Herrero, J.d.M. Munoz, S. Giordani, A. Diaz-Ortiz, S. Filippone, G. Ruaro, M. Meneghetti, M. Prato, E. Vazquez, J. Am. Chem. Soc. 129 (2007) 14580–14581.
[20] N. Nair, W.-J. Kim, M.L. Usrey, M.S. Strano, J. Am. Chem. Soc. 129 (2007) 3946–3954.
[21] K.V. Gothelf, K.A. Jorgensen, Chem. Rev. 98 (1998) 863–909.
[22] HyperChem, Hypercube Inc., Gainesville, Florida, USA.
[23] A. Suri, K.S. Coleman, Carbon 49 (2011) 3031–3038.
[24] M. Holzinger, J. Abraha, P. Whelan, R. Graupner, L. Ley, F. Hennrich, M. Kappes, A. Hirsch, J. Am. Chem. Soc. 125 (2003) 8566–8580.
[25] B.C. Wang, H.W. Wang, I.C. Lin, Y.S. Lin, Y.M. Chou, H.L. Chiu, J. Chin. Chem. Soc. 50 (2003) 939–945.
[26] T. Sato, M. Tanaka, T. Yamabe, Synth. Met. 103 (1999) 2525–2526.
[27] A. Rochefort, D.R. Salahub, P. Avouris, J. Phys. Chem. B 103 (1999) 641–646.
[28] K.N. Houk, J. Sims, R.E. Duke, R.W. Strozier, J.K. George, J. Am. Chem. Soc. 95 (1973) 7287–7301.
[29] K.N. Houk, J. Sims, C.R. Watts, L.J. Luskus, J. Am. Chem. Soc. 95 (1973) 7301–7315.
[30] R. Sustmann, Tetrahedron Lett. (1971) 2717–2720.
[31] G.E. Froudakis, Nano Lett. 1 (2001) 179–182.
[32] H.M. Wang, Y. Wang, K.L. Han, X.J. Peng, J. Org. Chem. 70 (2005) 4910–4917.
[33] K. Fukui, T. Yonezawa, C. Nagata, H. Shingu, J. Chem. Phys. 22 (1954) 1433.
[34] A. Hubbuch, R. Bindewald, J. Fohles, V.K. Naithani, H. Zahn, Angew. Chem. Int. Ed. Engl. 19 (1980) 394–396.
[35] S. Li, H. Kurtz, P. Korambath, Y.S. Li, J. Mol. Struct. 550 (2000) 235–244.
[36] A. Padwa, D.J. Austin, L. Precedo, L. Zhi, J. Org. Chem. 58 (1993) 1144–1150.
[37] H. Hu, B. Zhao, M.A. Hamon, K. Kamaras, M.E. Itkis, R.C. Haddon, J. Am. Chem. Soc. 125 (2003) 14893–14900.
[38] R. Saito, M. Fujita, G. Dresselhaus, M.S. Dresselhaus, Appl. Phys. Lett. 60 (1992) 2204–2206.
[39] P.J. Boul, J. Liu, E.T. Mickelson, C.B. Huffman, L.M. Ericson, I.W. Chiang, K.A. Smith, D.T. Colbert, R.H. Hauge, J.L. Margrave, R.E. Smalley, Chem. Phys. Lett. 310 (1999) 367–372.
[40] B.J. Landi, H.J. Ruf, J.J. Worman, R.P. Raffaelle, J. Phys. Chem. B 108 (2004) 17089–17095.
[41] N.O.V. Plank, R. Cheung, R.J. Andrews, Appl. Phys. Lett. 85 (2004) 3229–3231.
[42] N.O.V. Plank, L.D. Jiang, R. Cheung, Appl. Phys. Lett. 83 (2003) 2426–2428.

[43] C.M. Yang, K. Kaneko, M. Yudasaka, S. Iijima, Phys. B Condens. Matter 323 (2002) 140–142.
[44] J. Tarabek, L. Kavan, L. Dunsch, M. Kallbac, J. Phys. Chem. C 112 (2008) 13856–13861.
[45] L. Adams, A. Oki, T. Grady, H. McWhinney, Z. Luo, Phys. E Low Dimens. Syst. Nanostruct. 41 (2009) 723–728.
[46] A. Felten, C. Bittencourt, J.J. Pireaux, Nanotechnology 17 (2006) 1954–1959.
[47] K. Papagelis, M. Kalyva, D. Tasis, I. Parthenios, A. Siokou, C. Galiotis, Phys. Status Solidi B Basic Solid State Phys. 244 (2007) 4046–4050.
[48] S.V. Aradhya, S.V. Garimella, T.S. Fisher, J. Electrochem. Soc. 155 (2008) K161–K165.
[49] M.K. Rajumon, M.S. Hegde, C.N.R. Rao, Solid State Commun. 60 (1986) 267–270.
[50] M. Camalli, F. Caruso, G. Mattogno, E. Rivarola, Inorg. Chim. Acta 170 (1990) 225–231.
[51] K. Jurewicz, K. Babel, R. Pietrzak, S. Delpeux, H. Wachowska, Carbon 44 (2006) 2368–2375.
[52] D. Hulicova, J. Yamashita, Y. Soneda, H. Hatori, M. Kodama, Chem. Mater. 17 (2005) 1241–1247.
[53] M. Toupin, D. Belanger, J. Phys. Chem. C 111 (2007) 5394–5401.
[54] W.E. Swartz, K.J. Wynne, D.M. Hercules, Anal. Chem. 43 (1971) 1884–1887.
[55] J.C. Feng, G. Wen, W. Huang, E.T. Kang, K.G. Neoh, Polym. Degrad. Stab. 91 (2006) 12–20.
[56] Y. Cao, K.N. Houk, J. Mater. Chem. 21 (2011) 1503–1508.